HHS Public Access

Author manuscript

Adv Healthc Mater. Author manuscript; available in PMC 2018 August 23.

Published in final edited form as:

Adv Healthc Mater. 2018 August ; 7(16): e1800066. doi:10.1002/adhm.201800066.

Real-Time Imaging of Brain Tumor for Image-Guided Surgery

Dr. Shuang Hu,
Department of Nuclear Medicine, West China Hospital, Sichuan University, Chengdu 610041, China. Gordon Center for Medical Imaging, Department of Radiology, Massachusetts General Hospital and Harvard Medical School, Boston, MA 02114, USA

Dr. Homan Kang,
Gordon Center for Medical Imaging, Department of Radiology, Massachusetts General Hospital and Harvard Medical School, Boston, MA 02114, USA

Yoonji Baek,
Gordon Center for Medical Imaging, Department of Radiology, Massachusetts General Hospital and Harvard Medical School, Boston, MA 02114, USA

Prof. Georges El Fakhri,
Gordon Center for Medical Imaging, Department of Radiology, Massachusetts General Hospital and Harvard Medical School, Boston, MA 02114, USA

Prof. Anren Kuang, and
Department of Nuclear Medicine, West China Hospital, Sichuan University, Chengdu 610041, China

Prof. Hak Soo Choi
Gordon Center for Medical Imaging, Department of Radiology, Massachusetts General Hospital and Harvard Medical School, Boston, MA 02114, USA

Abstract

The completion of surgical resection is a key prognostic factor in brain tumor treatment. This requires surgeons to identify residual tumors in theater as well as to margin the proximity of the tumor to adjacent normal tissue. Subjective assessments, such as texture palpation or visual tissue differences, are commonly used by oncology surgeons during resection to differentiate cancer lesions from normal tissue, which can potentially result in either an incomplete tumor resection, or accidental removal of normal tissue. Moreover, malignant brain tumors are even more difficult to distinguish from normal brain tissue, and resecting noncancerous tissue may create neurological defects after surgery. To optimize the resection margin in brain tumors, a variety of intraoperative guidance techniques are developed, such as neuronavigation, magnetic resonance imaging, ultrasound, Raman spectroscopy, and optical fluorescence imaging. When combined with appropriate contrast agents, optical fluorescence imaging can provide the neurosurgeon real-time image guidance to improve resection completeness and to decrease surgical complications.

Correspondence to: Hak Soo Choi.

Conflict of Interest
The authors declare no conflict of interest.

Graphical abstract

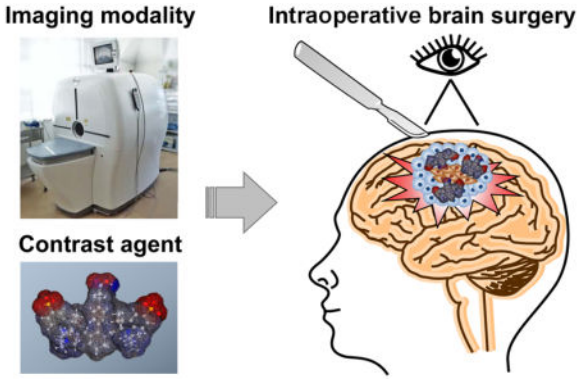

Keywords

brain tumors; contrast agents; image-guided therapy; intraoperative imaging; real-time imaging

1. Introduction

Glioblastoma multiforme (GBM) is the most aggressive form of malignant gliomas among adults.[1,2] Despite advances in chemotherapy, radiotherapy, and aggressive surgical resections, the prognosis of brain tumor remains poor.[3] Preoperative localization of cancers using conventional medical imaging increases the chances for successful treatments.[4,5] However, surgeons still suffer from the lack of intraoperative feedback that provides higher resolution and real-time image guidance without the risk associated with exposure to ionizing radiation to both the patient and surgeon. The completion of surgical resection demands the surgeon to accurately identify not only residual tumor in the field, but also the proximity of the tumor to adjacent normal tissue.[6,7] The estimated benefit of gross total resection is the extension of survival up to 14 months in glioblastoma and up to 90 months in low-grade glioma.[8]

Surgeons rely on subjective assessments (for example, texture palpation and visual tissue differences) during resection to distinguish cancer from near normal tissues, which may result in either incomplete tumor resection or unwarranted removal of normal tissue.[9,10] Furthermore, it is usually hard to differentiate malignant brain tumor from normal background tissue, and further resections might create neurological deficits after surgery. Since the brain parenchyma becomes distorted due to the loss of cerebrospinal fluid, edema, and tumor resection, the surgeon encounters hurdles.[11] Residual tumor tissue resides in 65–80% of glioma resections after surgery, highlighting the need for intraoperative imaging systems of malignant tissues.[7,12] For the investigation and delineation of brain tumors intraoperatively and thus optimize tumor resection, a variety of techniques such as neuronavigation system, intraoperative magnetic resonance imaging (iMRI), intraoperative ultrasound (iUS), intraoperative Raman spectroscopy (iRaman), and real-time optical fluorescence imaging (FLI) have been developed. The assistance of these modalities could possibly improve functional outcomes and decrease surgery-related complications, with or

without the combined contrast agents, by reserving critical structures and preventing the need for repeated surgeries, and reduce operating time and exposure to anesthesia.

2. Intraoperative Imaging Systems

2.1. Intraoperative Neuronavigation Systems

Neuronavigation refers to the computational process that integrates the pre- or intraoperative imaging data, and creates a translation map between imaging displayed on the screen (image space) and real spatial position (world space) to allow coregistration of imaging and patient anatomy.[13] It can then help the neurosurgeon to estimate the tumor margin and perform delicate resection, while the final point can be confirmed by further medical imaging. The workflow of a clinical neuronavigation system can be separated into four steps which are explained in detail in Figure 1.[14,15] The positional accuracy of a neuronavigation system is reported to be 2–3 mm. Moreover, the convenient integration of currently available and emerging multimodality imaging techniques, advanced MRI technologies, such as diffusion tensor imaging (DTI), MR spectroscopy, and fiber tracking, can also be imported and registered into the image data set.[16,17] This integrated data set also helps the precision of the system, prevents damage to the adjacent areas, and thus, improves the safety and efficacy of brain tumor surgery. This is a big advantage to neurosurgeons because such advanced imaging technologies cannot be applied during the surgery due to the requirement of field strength quality and proprocessing time. Neuronavigation system is also successful in reducing the length of surgery, giving the surgeons more confidence, lowering the incidence of wound infections, and shortening the length of hospital stay.[16,17]

However, the major challenge of this technique is the registration accuracy between preoperative images and intraoperative brain anatomy.[13] Since conventional navigation systems typically use medical images from preoperative imaging, the navigational accuracy is largely reduced by intraoperative brain shift due to cerebrospinal fluid loss, cyst decompression, cerebral edema, and parenchyma distortion during surgery.[20] Some neuronavigation systems attempt to include intraoperative imaging as an updated navigational database to maintain accurate navigation; however, problems in calculation and registration, as well as restrictions of space and view inside the operating field, make imperfect results.[21] Furthermore, the postprocessing of the images in neuronavigation systems, such as errors resulting from registration and fiber tracking, the lack of knowledge or caution of surgeons when displacing the skin-adhesive markers or moving the reference frame during surgery, could also increase the inaccuracy.[14] Emerging strategies for navigation, such as neuronavigated intraoperative microscopy, optical fluorescence imaging, and other molecular imaging should also be validated for clinical practice to examine their operational efficacy and cost efficiency.[22]

2.2. iMRI

MRI is the major modality of choice in diagnosing and defining tumor borders in the brain parenchyma. The rate of incorrect assumptions made by surgeons without the assistance of inter- or intraoperative system(s) about the extent of resections is strikingly high.[23] The brain shift caused by the loss of cerebrospinal fluid, edema, and tumor resection during

surgery makes the use of preoperative MRI for conventional neuronavigation less reliable for brain surgery.

Multiple studies showed a positive impact of intraoperative imaging on the extent of resection and outcome in brain tumor surgery.[23] Especially, iMRI demonstrated a dramatic improvement in the optimum extent of resection, quality of life, and survival in glioma patients.[24,25] A specific on-site “donut” MRI scanner (Figure 2a,c) or a parallel stationary MRI scanner in an adjacent room (Figure 2d) is needed to acquire data while the patient remains under anesthesia.[24,25] Acquisition of the iMRI provides real-time assessment of the tumor resection and allows further resection in the same operative session.[23] iMRI with functional MRI provides nearly real-time images with optimal quality, enabling neurosurgeons to selectively continue tumor resection, thus fully resecting the tumor while reducing the risk for neurological morbidity by allowing the surgeon to determine the relationships of the lesions to be resected to nearby critical brain structures (Figure 2b).[24]

Despite the strong clinical evidence, iMRI is associated with several drawbacks. Depending on the type of iMRI systems, the installation of a system costs about 3–8 million USD.[26] Additionally, neurosurgery with iMRI guidance is more time consuming, adding extra operation room (OR) time and cost to every procedure, and requires large operation space for the equipment and special MRI-compatible surgical instruments.[26] Senft et al. reported that an average of an additional 1 h was required for iMRI-involved neurosurgery compared to conventional surgery.[27] The problem with dose and timing of the contrast agent also affects the amount of residual enhancement, which influences the judgment of residual extent of the tumor.[26] In addition, advanced MR spectroscopy and DTI are restricted because of the relatively low magnetic field strength of most iMRI: only a cell density > 500 cells mm^{-1} is visible on the iMRI, and this restriction neglects invasive cancer cells. High-field iMRI with an integrated neuronavigation system is an advanced technical tool that is able to provide reliable anatomic and functional data during surgery; however, qualifying the cost-benefit issue is in need of active investigation.[28,29]

2.3. iUS

iUS provides an excellent true geometric position of a brain lesion and subsequently generates 2D or 3D images.[13] The data can be acquired in real time and reconstructed quickly and repeatedly at any time during surgery, allowing neurosurgeons to update operative plans without major workflow interruption.[13] iUS is often integrated with neuronavigation technology and enables side-by-side visualization of US with corresponding preoperative imaging.[30,31] However, the appearance of tissue from the 2D iUS depends on the frequency and angle of US waves; thus, it is challenging to interpret US images as well as to compare them with the imaging data from MR and CT (Figure 3a,b). 3D iUS can overcome this limitation by generating a volumetric image that can be viewed in any arbitrary plane, allowing registration with MRI images (Figure 3c–e). Despite these advantages in addition to real-time feedback without the use of ionizing radiation, the significance of iUS in routine clinical practice is not yet clearly defined: the quality of the images is subject to interoperator variability and motion artifacts, and low image resolution also restricts the application of ultrasonography in identifying the deep tumors.[31,32]

2.4. iRaman

Raman spectroscopy can give spectral tissue characteristics based on molecular vibrational information of chemical bonds resulting from the inelastic scattering of incident light.[31] This spectral information of the tissues, especially in the brain, can be identified, and relative molecular concentration of biological molecules can be evaluated to distinguish normal brain tissue from abnormal brain tissue. Jermyn et al. reported that the intra-operative system, which contained a fiber-coupled Raman spectrometer, successfully detected diffusely invasive brain cancer cells in patients with at least 90% accuracy for grade 2 to 4 gliomas (Figure 4).[33] The miniaturized handheld Raman probe operates in real time (acquisition time <0.2 s), making it convenient during the surgery with minimal disruption to the tumor resection procedure (Figure 4a). However, molecular footprint discrimination between cancerous and noncancerous tissue generally relies on complicated and robust machine-learning models that often discriminate based on very small spectral differences (Figure 4b).[34] It might result in failure to distinguish between different World Health Organization (WHO) grade invasive cancer cells in the normal brain or between grade 3 and 4 gliomas (accuracy, sensitivity, and specificity lower than 60%).

2.5. Intraoperative Optical FLI

Conventional neuronavigation system, iMRI or iUS, cannot achieve desirable images as easily as optical imaging because most contrast agents used for iMRI or iUS lack either high sensitivity or high specificity.[35] FLI using the near-infrared (NIR) fluorescence (650–900 nm) has been established as a powerful and promising tool to give surgeon real-time information about the location and margin of the tumor region by compensating the depth limitation up to 5 mm with the high signal-to-background ratio (SBR).[36–39] In addition, advantages of NIR-FLI are high sensitivity, lower cost, and a much less cumbersome detection instrumentation compared to other intraoperative imaging modalities. Furthermore, optical imaging systems do not use ionizing radiation and do not interface the surgical field because NIR light is invisible to the human eye.[40] However, some fundamental challenges faced by FLI are limited resolution, limited quantification, limited depth of penetration, and limited availability of targeted contrast agents.[41,42]

Figure 5a shows a schematic drawing of the FLARE imaging system, which is a compact, cart-based system that permits simultaneous and real-time acquisition of color video along with two independent channels of NIR fluorescent lights.[43] One NIR channel is centered at 700 nm emission, and another at 800 nm emission. NIR fluorescence excitation fluence rate is adjustable from 0 to 15 mW cm^{-2}, white light is provided at ≥40 000 lux, and camera exposure time is varied from 10 μs to 10 s. FLARE and mini-FLARE imaging systems meet all requirements of regulatory document AAMI/IEC #60601, which have been tested in clinical trials enrolling over 500 patients in the United States, the Netherlands, Japan, and Switzerland.[44] These FLARE imaging systems are relatively cheap and can be miniaturized to the desktop by integrating camera and optical filter sets.[41]

Although intraoperative optical imaging systems already exist in the clinic,[45,46] there is an ongoing need to develop high-affinity tumor targeting agents. Thus, development of NIR fluorophores that illuminate brain tumors with high sensitivity and high specificity after a

single intravenous injection is desperately needed (discussed in Section 3). Furthermore, because the imaging system has dual-NIR fluorescence channels, surrounding healthy brain and nervous tissues can be visualized simultaneously in addition to the tumor tissue, which reduces postoperative neurologic complications associated with intraoperative nerve damage.[47] Generally, optical fluorescence contrast agents with high specificity to organs/tumors are needed to separate the signal from either normal tissue or tissue autofluorescence. As shown in Figure 5b, signals in the brain of CD-1 mice and Yorkshire pigs can be clearly seen using wide field- and reflectance-based NIR fluorescence imaging system when brain permeable contrast agents were injected.

3. Contrast Agents for Optical Imaging

The contrast agent ideally should have a high tumor targeting specificity without changing the current surgical flow and last at least during the period of tumor resection and margin assessment, which is typically 1–4 h.[36,37] Targeting can be divided into two phases: organ-specific targeting (mode of action) and subcellular-specific targeting (mechanism of action).[48] Upon injection via various routes, targeted contrast agents travel the bloodstream and reach the brain tissue during the distribution-equilibrium phase (i.e., biodistribution), which plays a key role in the tumoral uptake of contrast agents. Subcellular targeting of the brain tumor is then followed by the mechanism of action based on the specificity of targeted agents. Regardless of molecular level affinity, however, a major challenge in molecular imaging is the delivery of targeted contrast agents to the target organs.[48] For brain tumor targeting in particular, contrast agents should diffuse/transport into brain tissue by passing the highly selective semipermeable blood–brain barrier (BBB).

There are three major approaches for tumor targeting: 1) passive targeting that utilizes the enhanced permeability and retention (EPR) effect to increase tumoral uptake nonspecifically, 2) active targeting that employs specific targeting ligands to label unique features on cancerous cells, and 3) activatable targeting that uses particular internal or external stimuli to activate the contrast agent on the specific target tissue (Figure 6).[49] The EPR effect refers to a phenomenon where large particles (e.g., biomolecules and nanoparticles) with hydrodynamic diameter (HD) ranging from 10 to 400 nm that can reach tumor tissues passively by extravasation from leaky vasculature, and then retain in the tumor beds due to reduced lymphatic drainage.[50] Although particle size plays a key role in EPR-based drug delivery, the size cutoff value for EPR is still controversial because tumor microenvironments (reviewed in ref. [51]) and other physicochemical factors also influence the tumor targeting efficacy such as molecular composition, shape, surface charge, hydrophilicity/lipophilicity, and charge-to-mass ratio (reviewed in ref. [52]). Indeed, Kobayashi et al. reported that nanoparticles larger than 6 nm in HD would have limited excretion by the kidneys and therefore, should provide longer circulation and EPR.[51]

Interestingly, such physicochemical rules can be applied to small particles with an HD less than 5.5 nm. We modulated the surface charges and lipophilicity of small molecule contrast agents, and such subtle changes in chemical structure resulted in large variations in their biodistribution, pharmacokinetics, and clearance in cells and animals.[53] In a separate study, we recently reported a comprehensive concept of the “small molecular EPR” using renal

clearable organic nanoparticles (a.k.a., H-Dots), which is composed of a biocompatible polymer with a charge-balanced surface.[54] H-Dots <5.5 nm in HD could deliver anticancer drugs to the tumor site with prolonged blood circulation without nonspecific uptake by the major immune system, followed by rapid renal clearance of untargeted agents from the body. This favorable biodistribution combined with the rapid renal clearance enhanced tumor targetability and reduced background uptake drastically, which together improved the final tumor-to-background ratio (TBR) over 24 h post-intravenous administration. This important concept was supported by Zheng and co-workers by using renal clearable gold nanoparticles that extravasated into the tumor bed and penetrated into various tumors in animal models through the small molecular EPR effect.[55,56]

EPR effect generally helps optical contrast agents to be retained in the tumor microenvironment for several days to weeks, this kind of contrast agent might cause high background signal outside the region of interest due to the lack of specificity. On the other hand, active targeting uses specific interactions between the targeting ligands, such as small molecules, peptides, antibodies, and aptamers, conjugating with optical contrast agents and cell surface markers specifically in cancer cells.[57] Therefore, the active targeting process should occur relatively fast with near complete excretion to obtain a high SBR.[58] For this reason, Choi et al. designed zwitterionic near-infrared fluorophores to conjugate with targeting ligands, which show ultralow serum binding, negligible nonspecific tissue background, and rapid elimination from the body through urinary excretion.[54,59–62]

Armed with a better understanding of the various biological response mechanisms, targeting agents that can be activated have been developed for minimizing background signal. These targeted agents exhibit diminished contrast before it is injected into the body, but become activated by physiological triggers associated with the tumor microenvironments such as pH, metabolite, enzyme, redox potential, or temperature after reaching the target tumor.[57,63] Although low background signal (inactivated area) resulting in ultrahigh SBR can be obtained, the triggered responses occur relatively slow in the body and accompany with nonspecific distribution. This could also increase potential toxicity because the inactivated contrast agents stay in the tissue and clear slowly through the hepatobiliary clearance.[57]

3.1. Food and Drug Administration (FDA)-Approved Fluorophores

There is a neurosurgical need for specific glioma-targeted contrast agents having a high TBR so that precise identification of the malignant tissue margin is possible. There are three FDA-approved fluorescent imaging agents mainly used in glioma surgery: sodium fluorescein, 5-aminolevulinic acid (5-ALA) with protoporphyrin IX (PplX), and indocyanine green (ICG).[64] The optical properties and injection information of these three agents with pros and cons are displayed in Table 1 and Figure 7.

3.1.1. Sodium Fluorescein—Sodium fluorescein has been used widely for retinal angiography and intracranial tumor resection since the 1940s, but it was finally approved by the US FDA in 2006 (Fluorescite; Alcon Research, Ltd.).[65] This green fluorophore delivers to the tumor site via broken BBB and accumulates in the malignant tumor nonspecifically through vascular leaking defects, pooling defects, and abnormal vasculature or

neovascularization.[64] Generally, modified microscopic equipment with a wavelength range of 560 nm is required to see the fluorescence, but no additional imaging device is required when used at high doses (5–10 mg kg^{-1}) during image-guided surgery because of its green color.[66] Fluorescent and nonfluorescent areas correlated with tumor–normal brain distinction was confirmed histologically with the sensitivity of 82–94% and the specificity of 90–95%.[67–69]

However, the intrinsic undesirable optical properties of fluorescein have been a challenge such as rapid photobleaching and autofluorescence from surrounding tissue.[64–66] In addition, high absorption and scattering of fluorescein result in the interrogation of only the surface layer, which reduces TBR and makes it difficult to use for cancer surgery.[65] Most importantly, the nonspecific accumulation in the tumor site and high background retention of fluorescein in normal brain areas are major disadvantages.[64] Schwake et al. closed a clinical trial using sodium fluorescein in glioma resection due to the limited correspondence between fluorescein and tumor tissue (i.e., low specificity) and the generally high level of fluorescence signal throughout the brain (i.e., high background).[70]

3.1.2. 5-ALA and PpIX—The use of 5-ALA for fluorescence-guided glioma resection was first approved in Europe (Gliolan, NX Development Corp.) in 2007, and is now approved in over 40 countries. In the US, Gliolan was filed for new drug application in 2016 as an optical imaging agent and approved in 2017 in high-grade glioma patients (WHO grade III or IV) as an adjunct for the visualization of malignant tissue during surgery.[71] 5-ALA is a natural biochemical precursor of hemoglobin that prompts the synthesis and accumulation of fluorescent porphyrins in malignant tumors.[72] Porphyrin fluorescence can be then excited by filtered light and visualized with a modified microscope.[73] Fluorescence-guided resection with 5-ALA achieved 29% reduction in the proportion of patients with residual high grade gliomas on early MRI and increased up to 6 months in progression-free survival compared to controls.[12] The typical dose of 5-ALA is 20 mg kg^{-1}, and the positive predictive value, specificity, and negative predictive value in high-grade gliomas are reported to be 92%, 77%, and 79%, respectively.[74] A randomized controlled multicenter phase III trial showed that patients who underwent surgery 5-ALA had significantly improved tumor resection and 6-month progression-free survival rates than patients who underwent conventional micro-surgery under white light.[12]

There are several limitations of using 5-ALA in brain tumor surgery. First, only 6% of grade II gliomas were positive for PpIX production after dosing (20 mg kg^{-1}) with the metabolic precursor 5-ALA compared to 57% positivity of grade III or grade IV gliomas.[75] Second, it is difficult to decide tumor margins after injection of 5-ALA because of vague fluorescence around the tumor site.[65] Nonspecific accumulations of PpIX in abscesses, metastases, necrotic tissues, and lymphomas result in such confusion during the tumor resection surgery.[76] Others have found that PpIX fluorescence is seen outside of tumor lesion which may cause unwarranted resection (false positive).[77] Nonspecific leakage of PpIX results in fluorescence detection in the peritumorous edema in a considerable number of cases, which limits patients to low-light conditions postoperatively to avoid associated phototoxicity.[76]

3.1.3. ICG—ICG was approved by the US FDA (IC-Green, Akorn, Inc.) in 1959 and has been tested in glioma angiography imaging.[78] The typical dose of ICG is 0.3 mg kg^{-1} and has been mainly used in cerebrovascular procedures to monitor blood flow during neurosurgery, resection of arteriovenous malformations, extracranial–intracranial bypass or aneurysm surgery.[79] The second window ICG signal correlates with the degree of gadolinium enhancement on MRI and also provides practical and sensitive means of identifying gliomas before dural opening as well as before corticectomy for accurate localization.[80] ICG accumulates into brain tumors nonspecifically through the EPR effect, but shows over 90% of specificity. Because autofluorescence is low in the NIR window (650–900 nm), the background signals are low, while NIR light shows low tissue absorption and scatter, enabling target detection up to 5 mm below the surface of the tissue.[40] Real-time ICG NIR imaging correlates with contrast enhancement on preoperative MRI scanning data and is able to identify tumor margin.[80]

However, ICG quickly accumulates into the liver within 5 min because of high lipophilicity and serum protein binding in the bloodstream, which increases liver toxicity and anaphylactic or urticarial reactions.[64] ICG accumulates in the lesion through EPR effect and is not tumor specific. Unspecific binding to proteins in vivo increases background fluorescence signal; even the autofluorescence is absent under NIR window. Rapid clearance of ICG ($t_{1/2} \leq 5$ min) requires continuous injection, which may exceed the lethal dose, limiting its use in the brain tumor surgery.[80]

3.2. Preclinical Targeted Contrast Agents

All the three clinically available fluorescence molecules discussed above are basically nonspecific to the brain tumor and do not provide real tumor targeting or distinct margins for precise resection. Novel targeted contrast agents that have better specificity to gliomas and that can also define tumor margins are needed for better clinical practice and output. Unfortunately, there is no targeted contrast agent clinically available for brain tumor imaging and surgery. These “smart” contrast agents achieve specific targeting either through active targeting by conjugation of fluorophores with tumor-specific ligands or activatable targeting by designing fluorophores to be activated in a specific tumor microenvironment (Figure 8).[57]

3.2.1. Small Molecule Fluorophores—Targeted small molecule ligands specific to brain tumors have been intensively investigated for clinical applications. For example, as shown in Figure 8, the first-in-human intraoperative tumor-specific fluorescence imaging was performed in ovarian cancer debulking surgery with systemically administered targeted fluorescent agent, folate-conjugated fluorescein isothiocyanate (folate–FITC).[36] Folate receptor-α (FR-α) is overexpressed in 90–95% of patients with epithelial ovarian cancer as well as other cancers including brain tumors.[81] Thus, FR-α is an attractive example of active targeting, but the use of folate–FITC in the intraoperative surgery has two main issues: first, overexpression of FR-α varies significantly between solid tumors originating from different organs, which limit the wide application of folate–FITC in other types of tumors including that from endometria, kidney, lung, mesothelioma, breast, and brain;[81] second, fluorescein is limited to use in the body because of autofluorescence as well as high

tissue absorption and scattering, while NIR light penetrates into deeper tissue up to 5 mm because of its effective attenuation coefficient and reasonable photon absorption by the NIR fluorophores (reviewed in ref. [40]). Therefore, more efforts are needed in development of tumor-specific targets with NIR fluorophores to assist surgeons in tumor resection.

Many preclinical efforts have also been made to use small molecule fluorophores specific to brain tumors for clinical translation. Neuropilin receptor (NRP1 or NRP2) is a vascular endothelial growth factor and significantly used tumor cell surface target, which plays a key role in tumor-mediated angiogenesis.[82] Wu et al. designed fluorescein- or radio-labeled tLyP-1 small peptides to target NRPs overexpressed in the gliomas and performed intraoperative tumor targeting in U87MG human glioma cell inoculated xenograft tumor mice.[82] Although high TBR (>3.4) was obtained 1 h postadministration, the brain tumor was located in the flank not in the brain, which diminished its clinical impact. Another example is a passive tumor targeting strategy using angiogenic tumor vasculature in the brain tumor. Recently, Dai and co-workers developed several novel fluorophores in the second NIR window region (NIR-II; 1000–1700 nm), which can dramatically increase feature clarity and penetration depths compared to shorter wavelength region (NIR-I window; 650–900 nm) for brain tumor imaging and image-guided cancer surgery.[83,84] Polyethylene glycol (PEG) modified NIR-II fluorophore (CH1055-PEG) was injected intravenously into U87MG brain tumor-bearing mice and showed passive tumoral uptake in the mouse glioblastoma, which was identified noninvasively through the intact scalp and skull at a depth of 4 mm (Figure 9).[84] The location of the brain tumor was identical with *T*2-color weighted MRI images followed by NIR-II imaging.

3.2.2. Tumor-Specific Antibody- or Peptide-Conjugated Fluorophores—

Epidermal growth factor receptor (EGFR), human epidermal growth factor receptor 2 (HER2), CD105, and vascular endothelial growth factor receptor (VEGFR) are often overexpressed in tumor cells and known as tumor targets which have been actively investigated in cell cultures and animal models of different tumor types. Therefore, many efforts have been made for tumor-specific active targeting using antibody-conjugated fluorophores specific to upregulated tumor biomarkers. These high affinity probes can highlight malignant tumors during surgical resection.[85–87] Cetuximab is a high affinity EGFR inhibitor and has been conjugated with various fluorophores for brain tumor targeting.[85] Pogue and co-workers conjugated IRDye 680RD–cetuximab and CW800–anti-EGFR affibody and compared their tumor binding affinity in xenograft brain tumor mice.[86] Both the antibody conjugates targeted gliomas successfully, but cetuximab uptake was found in the interior of tumors, while affibody was evenly dispersed throughout the tumor while showing the tumor margin more efficiently. Additionally, an NIR fluorophore (IRDye 800CW)-conjugated cetuximab was successfully used for fluorescence-guided resection of experimental malignant gliomas because of its significant high TBR (23.2 ± 5.1).[87] However, the nonspecific uptake of antibody-conjugated targeting agents in the major organs including liver, spleen, and lymph nodes has not been solved yet. To resolve this issue, Choi et al. conjugated a nonsticky zwitterionic NIR fluorophore (e.g., ZW800-1) on anti-HER2 monoclonal antibody, which showed superior HER2-specific targeting in human breast cancer specimen and xenograft tumor mice, while reducing non-specific uptake in the liver

and spleen significantly compared with CW800 or Cy5.5 conjugates.[59] HER2 is a transmembrane tyrosine kinase receptor and overexpresses in various tumors originating from breast, colon, bladder, ovary, lung, and glioblastoma.[88] This design strategy of conjugating zwitterionic NIR fluorophores on the surface of targeted antibody can overcome the general limitation of antibody-based cancer targeting, such as poor extravasation and nonspecific uptake resulting from macrophage recognition of circulating foreign materials.[48,89]

Although antibodies show great promise in tumor targeting, they are mostly bulky (e.g., IgG; 150 kDa, 11 nm in HD) and show unfavorable biodistribution.[90] Therefore, antibody-conjugated contrast agents exhibit limited BBB penetration and cellular uptake in vivo, while small peptides can overcome these limitations.[91] Chlorotoxin (CTX) and Arg-Gly-Asp peptide (RGD) are two major peptides conjugated with fluorophores and applied in brain imaging.[92–94] CTX is a 36-amino acid peptide and has three lysines at positions 15, 23, and 27 that act as potential sites for conjugation, while it shows specific and selective interactions with matrix metalloproteinase-2 (MMP-2), which is upregulated in gliomas and other tumors of the neuroectodermal origin but not expressed in normal brain.[95] Thus, CTX conjugates have been actively studied as imaging and therapeutic agents. For example, Cy5.5–CTX and ICG–CTX were used to identify brain tumor foci with high sensitivity as well as to define the tumor margins accurately in animal models.[92,96–98] Kobayashi et al. proved that Cy5.5–CTX targets intestinal cancers as well as prostate cancers and their small lymph node metastases,[92] while Olson and co-workers developed ICG–CTX for targeting canine soft tissue sarcoma and glioma with a high TBR.[99,100]

RDG-based peptides can bind and interfere with the cell adhesion molecule integrin $\alpha_v\beta_3$, which regulates tumor angiogenesis and its expression level and grade as well.[101,102] Since angiogenesis not only allows the growth of tumor but is also the way to metastasize, integrin $\alpha_v\beta_3$ is overexpressed on angiogenic blood vessels as well as the tumor cells in patients with glioblastoma.[101] Cy5.5–RGD successfully targeted integrin $\alpha_v\beta_3$ in xenograft and orthotopic animal models, but the uptake in the background tissue was relatively high.[103,104] As $\alpha_v\beta_3$ antagonist is currently being investigated as tumor-specific anticancer therapies,[102] isotope-labeled RDG can be used to quantify the response to such therapy.[105,106]

3.2.3. Activatable Fluorophores—An activatable targeting strategy is a smart approach that can maximize the TBR by decreasing background signals significantly, resulting in improving the tumor visibility in the margin during glioma surgery. Activatable fluorophores are complicated in design, meant to be activated in the target tissue microenvironment, where fluorescence turns on.[57] Although it requires highly intelligent molecular engineering technology, many researchers employ peptide-based activatable fluorescence probes that are based on the enzymatic cleavage by tumor-associated proteases.[107] Weissleder[108,109] and Tsien and co-workers[110,111] are pioneers in the development of the activatable fluorescence probes. Their innovating discovery and effort have yielded other groups applying these probes to the brain tumor imaging. For example, Cy5.5-labeled cathepsin-L cleavable probes was developed to target glioma cells with increased cathepsin-L activity.[112] Glioma targeting resulted in the rapid and robust identification of very small

tissue associated with protease activity because cathepsin is highly enzyme specific and forms a stable covalent bond after targeting.[113] This enzymatic characteristic also allowed topical application of the activatable probes to identify residual glioma cells after initial brain tumor resection.[112] However, despite high sensitivity and specificity, the result from the use of activatable contrast agents might vary due to the fluctuation of enzymatic activity in brain tumor patients.

4. Multimodal Brain Tumor Imaging

A wide variety of techniques have been explored in an effort to define the extent of tumor resection in human brain surgery. Despite broad ranged specificity and sensitivity, the gross total resection of high-grade gliomas using 5-ALA, sodium fluorescein, iMRI, and iUS was all similar: 69%, 84%, 70%, and 73%, respectively.[114] Interestingly, the incremental costs for the four different modalities were all under the threshold of cost effectiveness for high-grade glioma therapy.[71] This means combining these modalities, or even developing new modalities can be adopted for better surgical outcomes. The key to achieving total resection of gliomas is the clear delineation of tumor margins, but the modalities discussed above have a lack of histological correlation and have limited access to the cellular level. Along with this goal, a triple-modal MRI–photoacoustic–Raman nanoparticle was developed by Gambhir and co-workers (Figure 10).[115] MRI allows preoperative detection of trimodal nanoparticles in the brain, followed by surgical planning. The injected probes can stay in the brain tumor for several days and provide tumor-specific imaging during intraoperative surgery. Photoacoustic imaging can provide guidance for tumor resection due to its relatively high resolution and deep tissue penetration. Raman imaging can then be used for further removal of any residual microscopic tumor cells because of its ultrahigh sensitivity and spatial resolution. The resected specimen can be assessed using a Raman probe ex vivo subsequently to verify negative tumor margins (Figure 10a). Postinjection images of all the three modalities with clear tumor visualization (dashed boxes outline the imaged area) are shown in Figure 10b, and 3D rendering of MRI with the segmented tumor represents good colocalization (Figure 10c). Significant improvement in each imaging was achieved by injecting trimodal imaging probes, which was quantified in Figure 10d. Overall, this trimodal modality delineated the margins of brain tumors successfully preoperatively and intraoperatively in living mice. The combination of these trimodal imaging techniques with a smart nanoparticle yielded excellent results, and the MPR nanoparticle composed of gold–silica with minimum cytotoxicity may have a better chance for clinical translation.[115] However, the animal model used in this study was immune-deficient mice bearing orthotopic xenograft tumors in the brain. This animal model often overgrows tumors outside the brain, forming a pedunculated tumor with interrupted BBB, which makes nanoparticles easy to penetrate into the tumor site. In addition, U87MG tumor cells used in this study was found to be different from the original U87 tissue, suggesting a contamination, and the animal models used in this cell line are unlikely to be representative of the human disease.[116] Therefore, this imaging modality with the trimodal nanoparticle must be confirmed in other transgenic brain tumor animal models having early stage invasive tumors and representing more close human brain tumors before translating into the clinic.

5. Conclusions

The completion of surgical resection is undoubtedly a key prognostic factor in neuro-oncology. To do this, development of multimodal imaging systems and investigating new imaging modalities combined with appropriate targeted contrast agents for intraoperative human surgery are in desperate need. Future intraoperative imaging systems integrated with updated imaging data, iMRI, iUS, iRaman, functional MRI, positron emission tomography (PET) imaging, and possibly optical imaging would be a strong tool for better planning and executing safe, efficient interventions for brain tumors, especially those located in eloquent and skull base regions. In addition, discovering NIR fluorescent contrast agents targeted to brain tumors will open new possibilities for real-time tumor-specific fluorescence imaging in human.

Acknowledgments

S.H. and H.K. contributed equally to this work. The authors thank Ivey Choi for editing of the paper. This study was supported by the US NIH grant NIBIB #R01-EB022230, the Korean Marine Biotechnology Program #PJT200979 funded by the Ministry of Oceans and Fisheries, and the Chinese National Natural Science Foundation #81471692 and the China Scholarship Council.

References

1. Giraudeau C, Geffroy F, Meriaux S, Boumezbeur F, Robert P, Port M, Robic C, Le Bihan D, Lethimonnier F, Valette J. Angiogenesis. 2013; 16:171. [PubMed: 23053783]
2. Wen PY, Kesari S. N Engl J Med. 2008; 359:492. [PubMed: 18669428]
3. Wakimoto H, Kesari S, Farrell CJ, Curry WT, Zaupa C, Aghi M, Kuroda T, Stemmer-Rachamimov A, Shah K, Liu TC, Jeyaretna DS, Debasitis J, Pruszak J, Martuza RL, Rabkin SD. Cancer Res. 2009; 69:3472. [PubMed: 19351838]
4. Ottenhausen M, Krieg SM, Meyer B, Ringel F. Neurosurg Focus. 2015; 38:E3.
5. Petridis AK, Anokhin M, Vavruska J, Mahvash M, Scholz M. Clin Neurol Neurosurg. 2015; 131:64. [PubMed: 25704192]
6. Bucci MK. Cancer. 2004; 101:817. [PubMed: 15305415]
7. McGirt MJ, Chaichana KL, Attenello FJ, Weingart JD, Than K, Burger PC, Olivi A, Brem H, Quinones-Hinojosa A. Neurosurgery. 2008; 63:700. [PubMed: 18981880]
8. Sanai N, Berger MS. Neurotherapeutics. 2009; 6:478. [PubMed: 19560738]
9. Rosenthal EL, Warram JM, Bland KI, Zinn KR. Ann Surg. 2015; 261:46. [PubMed: 25599326]
10. Rosenthal EL, Warram JM, de Boer E, Basilion JP, Biel MA, Bogyo M, Bouvet M, Brigman BE, Colson YL, DeMeester SR, Gurtner GC, Ishizawa T, Jacobs PM, Keereweer S, Liao JC, Nguyen QT, Olson JM, Paulsen KD, Rieves D, Sumer BD, Tweedle MF, Vahrmeijer AL, Weichert JP, Wilson BC, Zenn MR, Zinn KR, van Dam GM. J Nucl Med. 2016; 57:144. [PubMed: 26449839]
11. Toms SA. Neurosurgery. 2005; 57:382. [PubMed: 16234690]
12. Stummer W. Lancet Oncol. 2006; 7:392. [PubMed: 16648043]
13. Barone DG, Lawrie TA, Hart MG. Cochrane Database Syst Rev. 2014:CD009685. [PubMed: 24474579]
14. Wang MN, Song ZJ. Neurosurgery. 2011; 68:1131. [PubMed: 21242841]
15. Gerard IJ, Kersten-Oertel M, Petrecca K, Sirhan D, Hall JA, Collins DL. Med Image Anal. 2017; 35:403. [PubMed: 27585837]
16. Mascott CR. J Neurosurg. 2006; 105:561. [PubMed: 17044559]
17. Watanabe Y, Hayashi Y, Fujii M, Kimura M, Sugiura A, Tsuzaka M, Wakabayashi T. Nihon Hoshasen Gijutsu Gakkai Zasshi. 2010; 66:131. [PubMed: 20203426]

18. Dlaka D, Svaco M, Chudy D, Jerbic B, Sekoranja B, Suligoj F, Vidakovic J, Almahariq F, Romic D. Int J Med Robotics Comput Assist Surg. 2018; 14:e1884.
19. Eyupoglu IY, Buchfelder M, Savaskan NE. Nat Rev Neurol. 2013; 9:141. [PubMed: 23358480]
20. Warfield SK, Haker SJ, Talos IF, Kemper CA, Weisenfeld N, Mewes AU, Goldberg-Zimring D, Zou KH, Westin CF, Wells WM. Med Image Anal. 2005; 9:145. [PubMed: 15721230]
21. Ferrant M, Nabavi A, Macq B, Black PM, Jolesz FA, Kikinis R, Warfield SK. Med Image Anal. 2002; 6:337. [PubMed: 12426109]
22. Orringer DA, Golby A, Jolesz F. Expert Rev Med Devices. 2012; 9:491. [PubMed: 23116076]
23. Black PM, Moriarty T, Alexander E, Stieg P, Woodard EJ, Gleason PL, Martin CH, Kikinis R, Schwartz RB, Jolesz FA. Neurosurgery. 1997; 41:831. [PubMed: 9316044]
24. Hall WA, Truwit CL. J Magn Reson Imaging. 2008; 27:368. [PubMed: 18183585]
25. Hlavac M, Wirtz CR, Halatsch ME. HNO. 2017; 65:25. [PubMed: 27670420]
26. Nimsky C. Lancet Oncol. 2011; 12:982. [PubMed: 21868283]
27. Senft C, Bink A, Franz K, Vatter H, Gasser T, Seifert V. Lancet Oncol. 2011; 12:997. [PubMed: 21868284]
28. Gil-Robles S, Duffau H. Neurosurg Focus. 2010; 28:E8.
29. Duffau H. World Neurosurg. 2014; 82:601. [PubMed: 24636939]
30. Gronningsaeter A, Kleven A, Ommedal S, Aarseth TE, Lie T, Lindseth F, Langø T, Unsgård G. Neurosurgery. 2000; 47:1373. [PubMed: 11126908]
31. Sastry R, Bi WL, Pieper S, Frisken S, Kapur T, Wells W 3rd, Golby AJ. J Neuroimaging. 2017; 27:5. [PubMed: 27541694]
32. Unsgaard G, Rygh OM, Selbekk T, Muller TB, Kolstad F, Lindseth F, Hernes TA. Acta Neurochir. 2006; 148:235. [PubMed: 16362178]
33. Jermyn M, Mok K, Mercier J, Desroches J, Pichette J, Saint-Arnaud K, Bernstein L, Guiot MC, Petrecca K, Leblond F. Sci Transl Med. 2015; 7:274ra19.
34. Laing S, Jamieson LE, Faulds K, Graham D. Nat Rev Chem. 2017; 1:0060.
35. Tichauer KM, Wang Y, Pogue BW, Liu JT. Phys Med Biol. 2015; 60:R239. [PubMed: 26134619]
36. van Dam GM, Themelis G, Crane LM, Harlaar NJ, Pleijhuis RG, Kelder W, Sarantopoulos A, de Jong JS, Arts HJ, van der Zee AG, Bart J, Low PS, Ntziachristos V. Nat Med. 2011; 17:1315. [PubMed: 21926976]
37. Nguyen QT, Tsien RY. Nat Rev Cancer. 2013; 13:653. [PubMed: 23924645]
38. Vahrmeijer AL, Hutteman M, van der Vorst JR, van de Velde CJ, Frangioni JV. Nat Rev Clin Oncol. 2013; 10:507. [PubMed: 23881033]
39. van der Vorst JR, Schaafsma BE, Hutteman M, Verbeek FP, Liefers GJ, Hartgrink HH, Smit VT, Lowik CW, van de Velde CJ, Frangioni JV, Vahrmeijer AL. Cancer. 2013; 119:3411. [PubMed: 23794086]
40. Owens EA, Lee S, Choi J, Henary M, Choi HS. Wiley Interdiscip Rev: Nanomed Nanobiotechnol. 2015; 7:828. [PubMed: 25645081]
41. Kim TH, O'Brien C, Choi HS, Jeong MY. Appl Spectrosc Rev. 2018; 53:349.
42. Park GK, HI, Kim GS, Hwang NS, Choi HS. Appl Spectrosc Rev. 2018; 53:360. [PubMed: 29563664]
43. Troyan SL, Kianzad V, Gibbs-Strauss SL, Gioux S, Matsui A, Oketokoun R, Ngo L, Khamene A, Azar F, Frangioni JV. Ann Surg Oncol. 2009; 16:2943. [PubMed: 19582506]
44. Burrington DJ. BioOptics World. PennWell Corporation; Tulsa, OK, USA: 2015. Fluorescence-Guided Surgery: Advanced Surgery: NIR Fluorescence Guidance Arrives.
45. Gioux S, Choi HS, Frangioni JV. Mol Imaging. 2010; 9:237. [PubMed: 20868625]
46. Venugopal V, Park M, Ashitate Y, Neacsu F, Kettenring F, Frangioni JV, Gangadharan SP, Gioux S. J Biomed Opt. 2013; 18:126018. [PubMed: 24362927]
47. Park MH, Hyun H, Ashitate Y, Wada H, Park G, Lee JH, Njiojob C, Henary M, Frangioni JV, Choi HS. Theranostics. 2014; 4:823. [PubMed: 24955143]
48. Lee JH, Park G, Hong GH, Choi J, Choi HS. Quant Imaging Med Surg. 2012; 2:266. [PubMed: 23289086]

49. Maeda H, Wu J, Sawa T, Matsumura Y, Hori K. J Controlled Release. 2000; 65:271.
50. Nakamura Y, Mochida A, Choyke PL, Kobayashi H. Bioconjugate Chem. 2016; 27:2225.
51. Kobayashi H, Watanabe R, Choyke PL. Theranostics. 2013; 4:81. [PubMed: 24396516]
52. Choi HS, Frangioni JV. Mol Imaging. 2010; 9:291. [PubMed: 21084027]
53. Koo H, Lee JH, Bao K, Wu Y, El Fakhri G, Henary M, Yun SH, Choi HS. Adv Healthcare Mater. 2016; 5:2510.
54. Kang H, Gravier J, Bao K, Wada H, Lee JH, Baek Y, El Fakhri G, Gioux S, Rubin BP, Coll JL, Choi HS. Adv Mater. 2016; 28:8162. [PubMed: 27414255]
55. Du B, Jiang X, Das A, Zhou Q, Yu M, Jin R, Zheng J. Nat Nanotechnol. 2017; 12:170. [PubMed: 27842065]
56. Xu J, Yu M, Carter P, Hernandez E, Dang A, Kapur P, Hsieh JT, Zheng J. Angew Chem, Int Ed. 2017; 56:13356.
57. Owens EA, Henary M, El Fakhri G, Choi HS. Acc Chem Res. 2016; 49:1731. [PubMed: 27564418]
58. Bertrand N, Wu J, Xu X, Kamaly N, Farokhzad OC. Adv Drug Delivery Rev. 2014; 66:2.
59. Choi HS, Gibbs SL, Lee JH, Kim SH, Ashitate Y, Liu F, Hyun H, Park G, Xie Y, Bae S, Henary M, Frangioni JV. Nat Biotechnol. 2013; 31:148. [PubMed: 23292608]
60. Choi HS, Nasr K, Alyabyev S, Feith D, Lee JH, Kim SH, Ashitate Y, Hyun H, Patonay G, Strekowski L, Henary M, Frangioni JV. Angew Chem, Int Ed Engl. 2011; 50:6258. [PubMed: 21656624]
61. Hyun H, Henary M, Gao T, Narayana L, Owens EA, Lee JH, Park G, Wada H, Ashitate Y, Frangioni JV, Choi HS. Mol Imaging Biol. 2016; 18:52. [PubMed: 26084246]
62. Choi HS, Liu W, Misra P, Tanaka E, Zimmer JP, Itty Ipe B, Bawendi MG, Frangioni JV. Nat Biotechnol. 2007; 25:1165. [PubMed: 17891134]
63. Urano Y, Asanuma D, Hama Y, Koyama Y, Barrett T, Kamiya M, Nagano T, Watanabe T, Hasegawa A, Choyke PL, Kobayashi H. Nat Med. 2009; 15:104. [PubMed: 19029979]
64. Manrique-Guzman S, Herrada-Pineda T, Revilla-Pacheco F. Glioblastoma. DeVleeschouwer S, editorCodon Publications; Brisbane (AU): 2017.
65. Li Y, Rey-Dios R, Roberts DW, Valdes PA, Cohen-Gadol AA. World Neurosurg. 2014; 82:175. [PubMed: 23851210]
66. Shinoda J, Yano H, Yoshimura SI, Okumura A, Kaku Y, Iwama T, Sakai N. J Neurosurg. 2003; 99:597. [PubMed: 12959452]
67. Acerbi F, Broggi M, Eoli M, Anghileri E, Cavallo C, Boffano C, Cordella R, Cuppini L, Pollo B, Schiariti M. Neurosurg Focus. 2014; 36:E5.
68. Diaz RJ, Dios RR, Hattab EM, Burrell K, Rakopoulos P, Sabha N, Hawkins C, Zadeh G, Rutka JT, Cohen-Gadol AA. J Neurosurg. 2015; 122:1360. [PubMed: 25839919]
69. Martirosyan NL, Eschbacher JM, Kalani MYS, Turner JD, Belykh E, Spetzler RF, Nakaji P, Preul MC. Neurosurg Focus. 2016; 40:E11.
70. Schwake M, Stummer W, Molina EJS, Wölfer J. Acta Neurochir. 2015; 157:877. [PubMed: 25820632]
71. Catapano G, Sgulo FG, Seneca V, Lepore G, Columbano L, di Nuzzo G. World Neurosurg. 2017; 104:239. [PubMed: 28512039]
72. Míkvy P, Messmann H, Regula J, Conio M, Pauer M, Millson C, MacRobert A, Bown S. Neoplasma. 1995; 42:109. [PubMed: 7637818]
73. Stummer W. Neurosurgery. 2016; 78:484. [PubMed: 26552043]
74. Cui JT, Zhang HZ, Bu JQ, Chen P, Xi Q, Bu RF. Zhonghua Yi Xue Za Zhi. 2012; 92:1416. [PubMed: 22883202]
75. Floeth FW, Sabel M, Ewelt C, Stummer W, Felsberg J, Reifenberger G, Steiger HJ, Stoffels G, Coenen HH, Langen KJ. Eur J Nucl Med Mol Imaging. 2011; 38:731. [PubMed: 21153408]
76. Roberts DW, Valdés PA, Harris BT, Fontaine KM, Hartov A, Fan X, Ji S, Lollis SS, Pogue BW, Leblond F, Tosteson TD, Wilson BC, Paulsen KD. J Neurosurg. 2011; 114:595. [PubMed: 20380535]

77. Kamp MA, Felsberg J, Sadat H, Kuzibaev J, Steiger HJ, Rapp M, Reifenberger G, Dibué M, Sabel M. Acta Neurochir. 2015; 157:207. [PubMed: 25547719]
78. Haglund MM, Berger MS, Hochman DW. Neurosurgery. 1996; 38:308. [PubMed: 8869058]
79. Raabe A, Beck J, Gerlach R, Zimmermann M, Seifert V. Neurosurgery. 2003; 52:132. [PubMed: 12493110]
80. Lee JYK, Thawani JP, Pierce J, Zeh R, Martinez-Lage M, Chanin M, Venegas O, Nims S, Learned K, Keating J, Singhal S. Neurosurgery. 2016; 79:856. [PubMed: 27741220]
81. Parker N, Turk MJ, Westrick E, Lewis JD, Low PS, Leamon CP. Anal Biochem. 2005; 338:284. [PubMed: 15745749]
82. Wu H-bWang Z, Wang Q-sHan Y-jWang M, Zhou W-lLi H-s. PLoS One. 2015; 10:e0137676. [PubMed: 26398657]
83. Hong G, Diao S, Chang J, Antaris AL, Chen C, Zhang B, Zhao S, Atochin DN, Huang PL, Andreasson KI, Kuo CJ, Dai H. Nat Photonics. 2014; 8:723. [PubMed: 27642366]
84. Antaris AL, Chen H, Cheng K, Sun Y, Hong G, Qu C, Diao S, Deng Z, Hu X, Zhang B, Zhang X, Yaghi OK, Alamparambil ZR, Hong X, Cheng Z, Dai H. Nat Mater. 2016; 15:235. [PubMed: 26595119]
85. Goldstein NI, Prewett M, Zuklys K, Rockwell P, Mendelsohn J. Clin Cancer Res. 1995; 1:1311. [PubMed: 9815926]
86. Sexton K, Tichauer K, Samkoe KS, Gunn J, Hoopes PJ, Pogue BW. PLoS One. 2013; 8:e60390. [PubMed: 23593208]
87. Warram JM, de Boer E, Korb M, Hartman Y, Kovar J, Markert JM, Gillespie GY, Rosenthal EL. Br J Neurosurg. 2015; 29:850. [PubMed: 26073144]
88. Ruan J, Song H, Qian Q, Li C, Wang K, Bao C, Cui D. Biomaterials. 2012; 33:7093. [PubMed: 22796163]
89. Choi HS, Liu W, Liu F, Nasr K, Misra P, Bawendi MG, Frangioni JV. Nat Nanotechnol. 2010; 5:42. [PubMed: 19893516]
90. Kobayashi H, Hama Y, Koyama Y, Barrett T, Regino CA, Urano Y, Choyke PL. Nano Lett. 2007; 7:1711. [PubMed: 17530812]
91. Aina OH, Sroka TC, Chen ML, Lam KS. Biopolymers. 2002; 66:184. [PubMed: 12385037]
92. Veiseh M, Gabikian P, Bahrami SB, Veiseh O, Zhang M, Hackman RC, Ravanpay AC, Stroud MR, Kusuma Y, Hansen SJ, Kwok D, Munoz NM, Sze RW, Grady WM, Greenberg NM, Ellenbogen RG, Olson JM. Cancer Res. 2007; 67:6882. [PubMed: 17638899]
93. Shen S, Khazaeli M, Gillespie GY, Alvarez VL. J Neuro-Oncol. 2005; 71:113.
94. Chen X, Tohme M, Park R, Hou Y, Bading JR, Conti PS. Mol Imaging. 2004; 3:96. [PubMed: 15296674]
95. DeBin J, Strichartz G. Toxicon. 1991; 29:1403. [PubMed: 1726031]
96. Akcan M, Stroud MR, Hansen SJ, Clark RJ, Daly NL, Craik DJ, Olson JM. J Med Chem. 2011; 54:782. [PubMed: 21210710]
97. Veiseh O, Sun C, Gunn J, Kohler N, Gabikian P, Lee D, Bhattarai N, Ellenbogen R, Sze R, Hallahan A. Nano Lett. 2005; 5:1003. [PubMed: 15943433]
98. Butte PV, Mamelak A, Parrish-Novak J, Drazin D, Shweikeh F, Gangalum PR, Chesnokova A, Ljubimova JY, Black K. Neurosurg Focus. 2014; 36:E1.
99. Fidel J, Kennedy KC, Dernell WS, Hansen S, Wiss V, Stroud MR, Molho JI, Knoblaugh SE, Meganck J, Olson JM, Rice B, Parrish-Novak J. Cancer Res. 2015; 75:4283. [PubMed: 26471914]
100. Stroud MR, Hansen SJ, Olson JM. Curr Pharm Des. 2011; 17:4362. [PubMed: 22204434]
101. Bello L, Francolini M, Marthyn P, Zhang J, Carroll RS, Nikas DC, Strasser JF, Villani R, Cheresh DA, Black PM. Neurosurgery. 2001; 49:380. [PubMed: 11504114]
102. Desgrosellier JS, Cheresh DA. Nat Rev Cancer. 2010; 10:9. [PubMed: 20029421]
103. Cheng Z, Wu Y, Xiong Z, Gambhir SS, Chen X. Bioconjugate Chem. 2005; 16:1433.
104. Hsu AR, Hou LC, Veeravagu A, Greve JM, Vogel H, Tse V, Chen X. Mol Imaging Biol. 2006; 8:315. [PubMed: 17053862]

105. Haubner R, Weber WA, Beer AJ, Vabuliene E, Reim D, Sarbia M, Becker KF, Goebel M, Hein R, Wester HJ, Kessler H, Schwaiger M. PLoS Med. 2005; 2:e70. [PubMed: 15783258]
106. Chen X, Hou Y, Tohme M, Park R, Khankaldyyan V, Gonzales-Gomez I, Bading JR, Laug WE, Conti PS. J Nucl Med. 2004; 45:1776. [PubMed: 15471848]
107. Tung CH. Biopolymers. 2004; 76:391. [PubMed: 15389488]
108. Weissleder R. Nat Biotechnol. 2001; 19:316. [PubMed: 11283581]
109. Bremer C, Tung CH, Weissleder R. Nat Med. 2001; 7:743. [PubMed: 11385514]
110. Chen B, Friedman B, Whitney MA, Van Winkle JA, Lei IF, Olson ES, Cheng Q, Pereira B, Zhao L, Tsien RY. J Neurosci. 2012; 32:7622. [PubMed: 22649241]
111. Chen S, Cui J, Jiang T, Olson ES, Cai QY, Yang M, Wu W, Guthrie JM, Robertson J, Lipton SA. J Cereb Blood Flow Metab. 2017; 37:188. [PubMed: 26681768]
112. Cutter JL, Cohen NT, Wang J, Sloan AE, Cohen AR, Panneerselvam A, Schluchter M, Blum G, Bogyo M, Basilion JP. PLoS One. 2012; 7:e33060. [PubMed: 22427947]
113. Heal WP, Dang TH, Tate EW. Chem Soc Rev. 2011; 40:246. [PubMed: 20886146]
114. Eljamel MS, Mahboob SO. Photodiagn Photodyn Ther. 2016; 16:35.
115. Kircher MF, de la Zerda A, Jokerst JV, Zavaleta CL, Kempen PJ, Mittra E, Pitter K, Huang RM, Campos C, Habte F, Sinclair R, Brennan CW, Mellinghoff IK, Holland EC, Gambhir SS. Nat Med. 2012; 18:829. [PubMed: 22504484]
116. Allen M, Bjerke M, Edlund H, Nelander S, Westermark B. Sci Transl Med. 2016; 8:354re3.

Biographies

Shuang Hu received her medical degree in Radiology and Nuclear Medicine from the West China School of Medicine, West China Hospital, Sichuan University in China. She is currently pursuing her Ph.D. at the Massachusetts General Hospital (MGH) and the Harvard Medical School in Boston, MA through the global joint program of the Sichuan University, where she expects to receive a Ph.D. in 2018. Her research focuses on the advanced clinical imaging and clinical translation of novel targeted molecular imaging for cancer theranostics.

Homan Kang is an Instructor in the Department of Radiology at the Harvard Medical School and Assistant Chemist at the Gordon Center for Medical Imaging (GCMI) of the MGH. He focuses on the development of novel targeted nanocarriers based on organic and inorganic nanostructures for theranostic drug delivery in Bioengineering & Nanomedicine Program at the GCMI.

Hak Soo Choi is an Associate Professor of Radiology at the Harvard Medical School, Associate Chemist at the MGH, and faculty of the Dana Farber/Harvard Cancer Center. Choi is currently Director of Bioengineering & Nanomedicine Program of the MGH GCMI. His laboratory focuses on the development of novel targeted contrast agents for image-guided surgical interventions to solve important problems in oncology and biomedical research, with an emphasis on molecular imaging and tissue-specific targeting.

Figure 1.

Neuronavigation workflow. 1) Prescanning of patient for neuronavigation using medical imaging. 2) Surgical planning by importing the medical images into the neuronavigation system. 3) Registration of the image space with the patient space. 4) Overlaying virtual surgical tools on the images transformed from the patient space into the images space. Reproduced with permission.[18] Copyright 2017, John Wiley & Sons. Reproduced with permission.[19] Copyright 2013, Springer Nature.

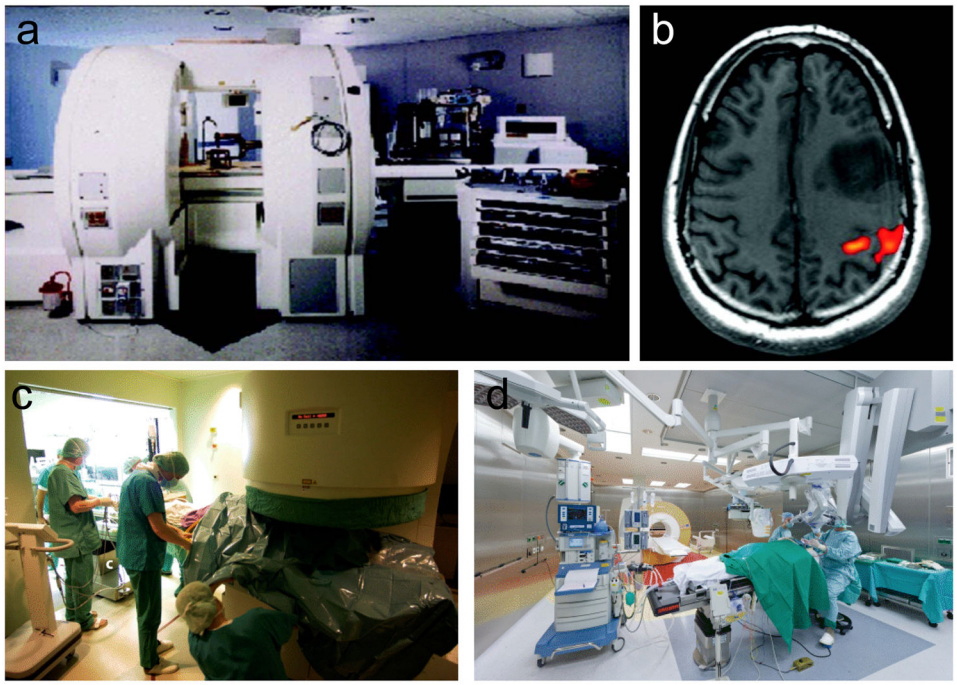

Figure 2.

Intraoperative MR-guided neurosurgery. a) 0.5 T Double coil design iMRI system. b) Activated brain area showing the motor cortex after finger tapping. Reproduced with permission.[24] Copyright 2008, John Wiley & Sons. c) Intraoperative installation of 0.2 T Siemens Magnetom Open. d) Brain tumor surgery in the integrated iMRI hybrid operating room. Reproduced with permission.[25] Copyright 2017, Springer Nature.

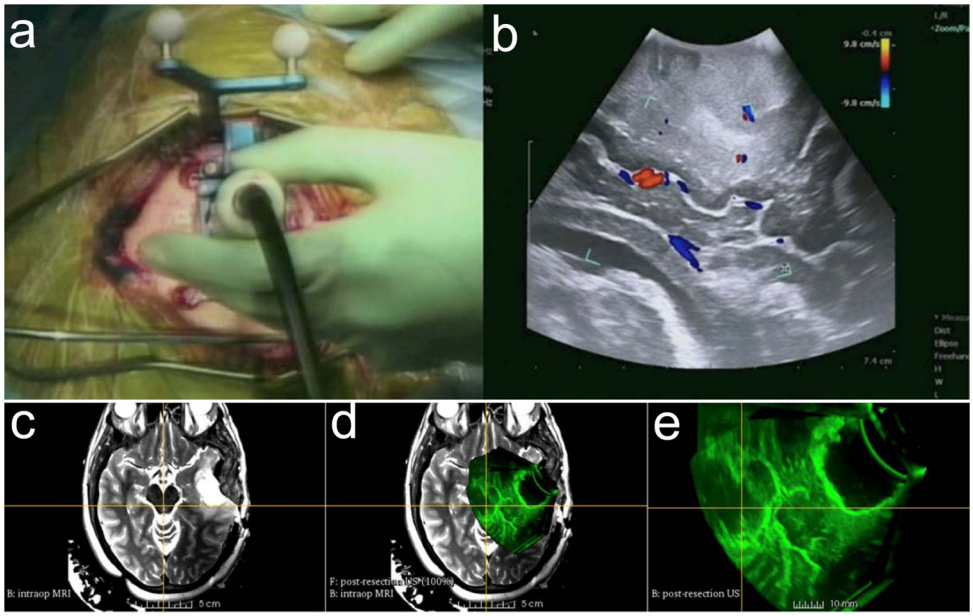

Figure 3.

Intraoperative ultrasound. a) Intraoperative 2D color Doppler ultrasound during tumor resection. b) 2D ultrasound image with superimposed color Doppler imaging. c) Intraoperative *T*2-FLAIR MRI after initial tumor resection. d) Coregistered image of intraoperative 3D US and intraoperative *T*2-FLAIR MRI. e) Intraoperative 3D US after initial tumor resection at the advanced multimodality image guided operating (AMIGO) suite at Brigham and Women's Hospital. Reproduced with permission.[31] Copyright 2017, John Wiley & Sons.

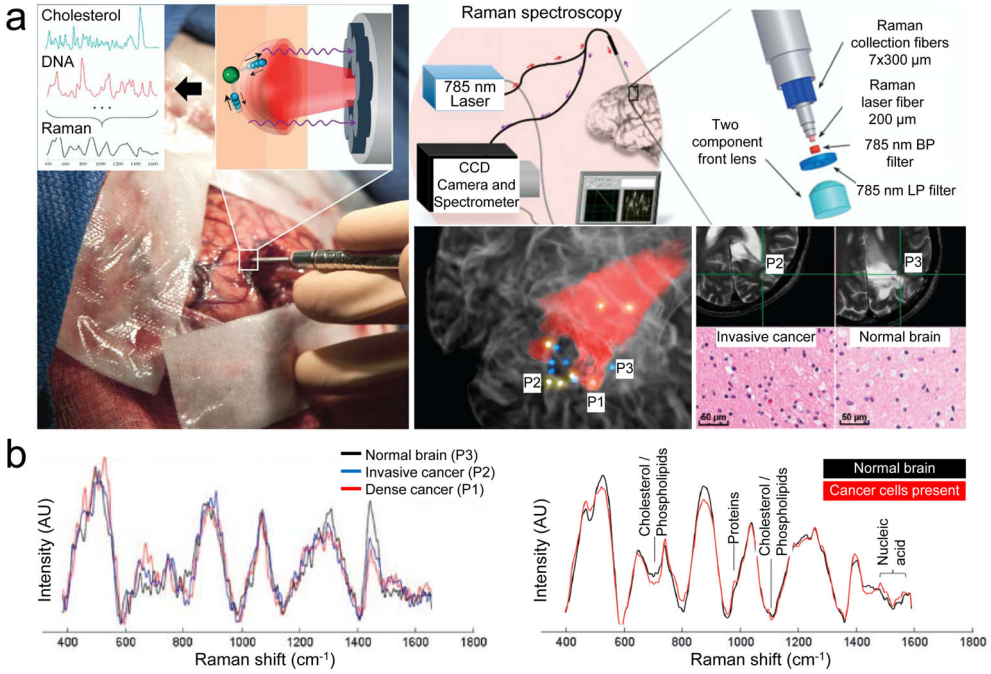

Figure 4.

The handheld contact fiber optic probe for Raman spectroscopy during glioma surgery collocated on preoperative MRI. a) The spectral differences occur owing to the vibrational modes of various molecular species, including cholesterol and DNA. Regions associated with colored dots were interrogated by Raman spectroscopy and were histologically analyzed: yellow indicates the presence of cancer cells; blue for negative cancer cells. P1, P2, and P3 are dense cancer, invasive cancer, and normal brain tissue, respectively. b) Raman spectra acquired for P1–P3 (left) and for discrimination of cancer tissue (right). The corresponding molecular contributors are identified for the most significant differences between the spectra for normal and cancer tissues. CCD, charge coupled device; BP, band-pass; LP, long-pass; AU, arbitrary unit. Reproduced with permission.[33] Copyright 2015, American Association for the Advancement of Science.

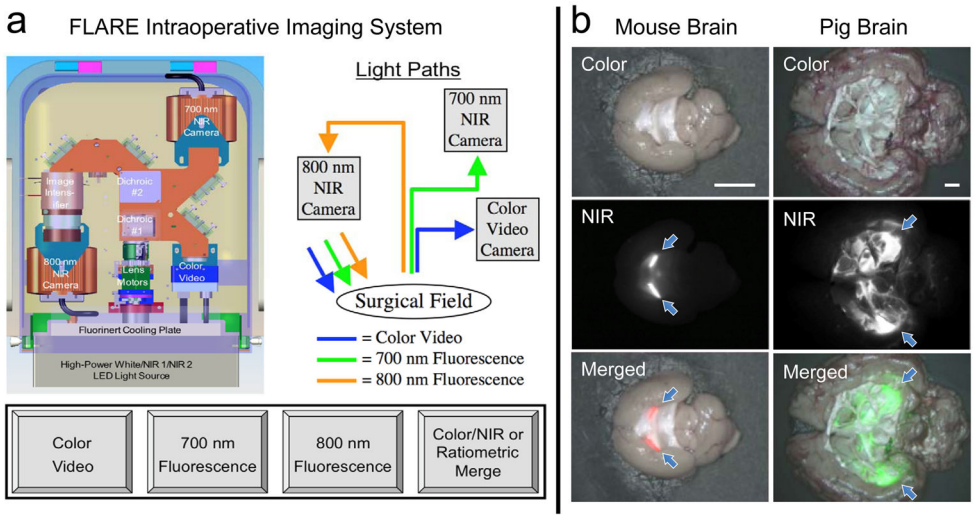

Figure 5.

Intraoperative optical fluorescence imaging. a) Schematic drawing and optical paths of the FLARE imaging platform. Color video (400–650 nm) and two independent channels (700/800 nm) of NIR fluorescence images are acquired simultaneously with custom software over a 15 cm diameter field of view. Reproduced with permission.[43] Copyright 2009, Springer Nature. b) NIR imaging of resected mouse brain (left, 700 nm) and pig brain (right, 800 nm). Imaged in color and NIR fluorescence under the FLARE imaging system. Red and lime green pseudocolors were used for 700 and 800 nm NIR in the merged image, respectively. Arrows = choroid plexus. Scale bars = 5 mm.

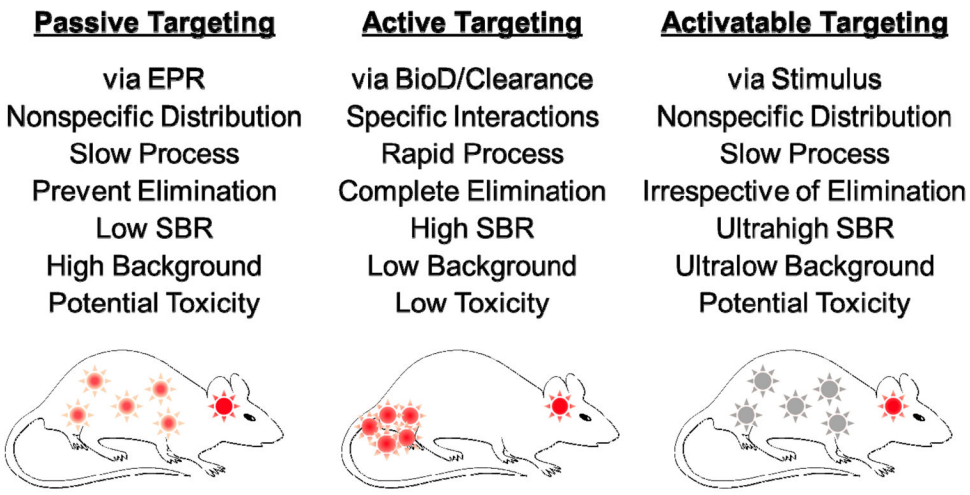

Figure 6.

Major strategies for brain tumor targeting: 1) passive targeting, 2) active targeting, 3) activatable targeting. Reproduced with permission.[57] Copyright 2015, American Chemical Society.

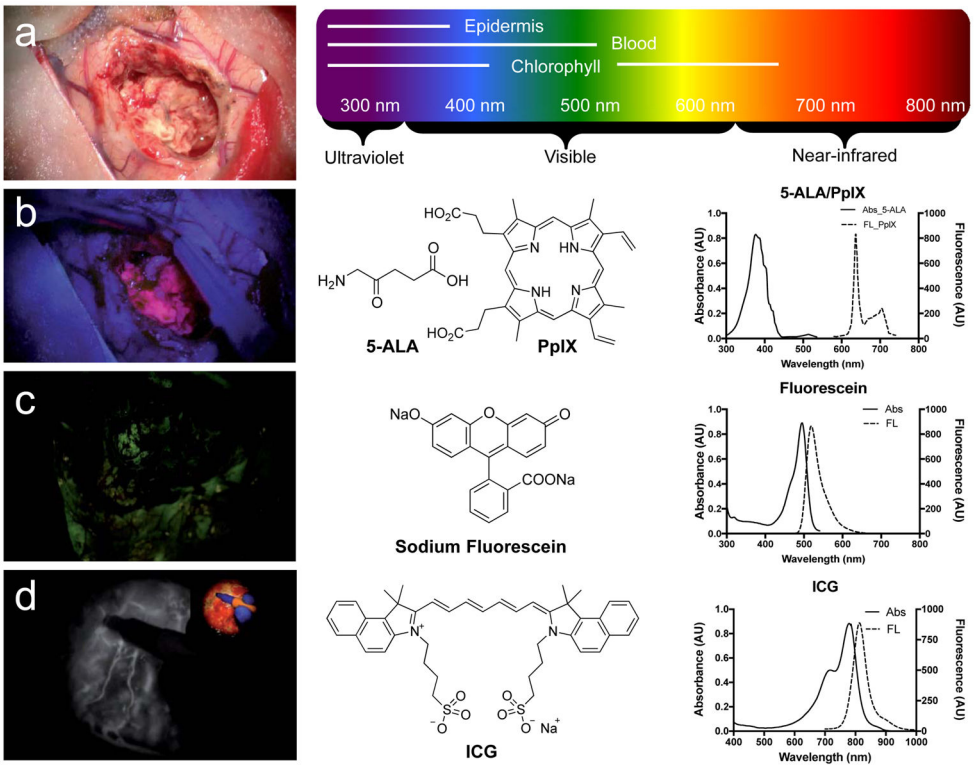

Figure 7.

Intraoperative brain tumor resection with the assistance of fluorophores. a) Regular white light. b) Blue light excitation (400 nm) using 5-ALA and PpIX. c) Green light excitation (500 nm) using fluorescein. d) NIR light excitation (800 nm) using ICG. Reproduced with permission.[64] Copyright 2017, Codon Publications.

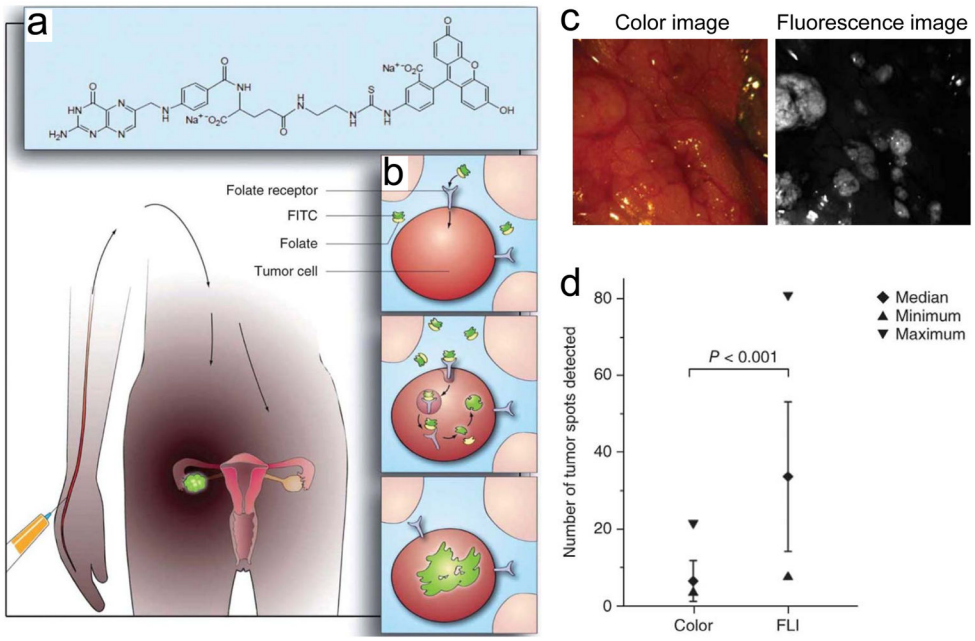

Figure 8.

Tumor-specific fluorescent agent. a) Folate is conjugated to fluorescein isothiocyanate (FITC). b) Schematic drawing of ovarian cancer targeting using folate–FITC. c) Color and fluorescence images of the abdominal cavity. d) Ex vivo quantitative scoring of tumor deposits. $p < 0.001$ by five independent surgeons. Reproduced with permission.[36] Copyright 2011, Springer Nature.

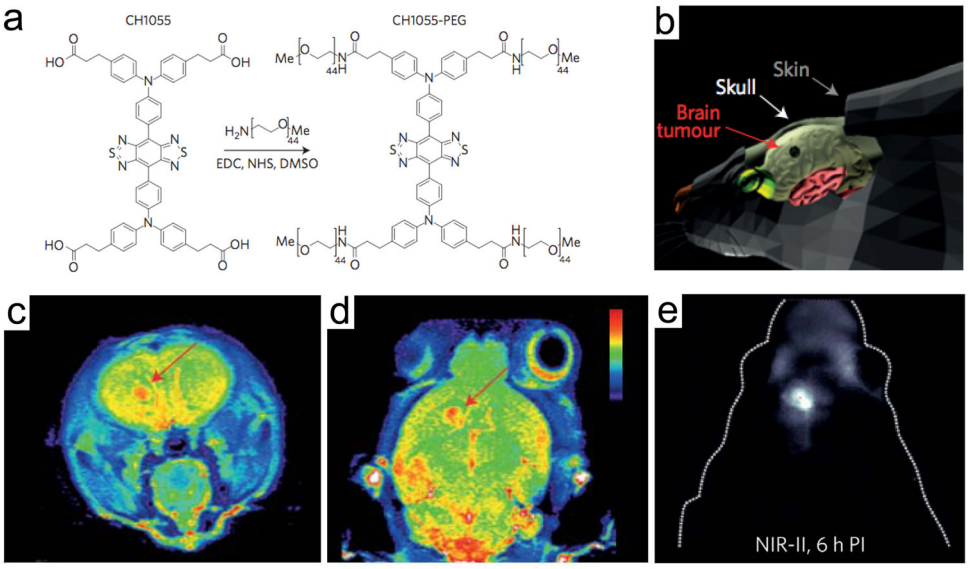

Figure 9.

Glioblastoma imaging in the NIR-II window. a) Chemical structure of PEGylated NIR fluorophore, CH1055-PEG. b) Schematic drawing for the location of U87MG orthotopic glioblastoma. *T*2-color weighted MRI images in the c) sagittal and d) coronal planes showing the implanted U87MG brain tumors (red arrows). e) High-magnified NIR-II fluorescence image of mouse brain through the scalp and skull 6 h post-intravenous injection of CH1055-PEG. Reproduced with permission.[84] Copyright 2016, Springer Nature.

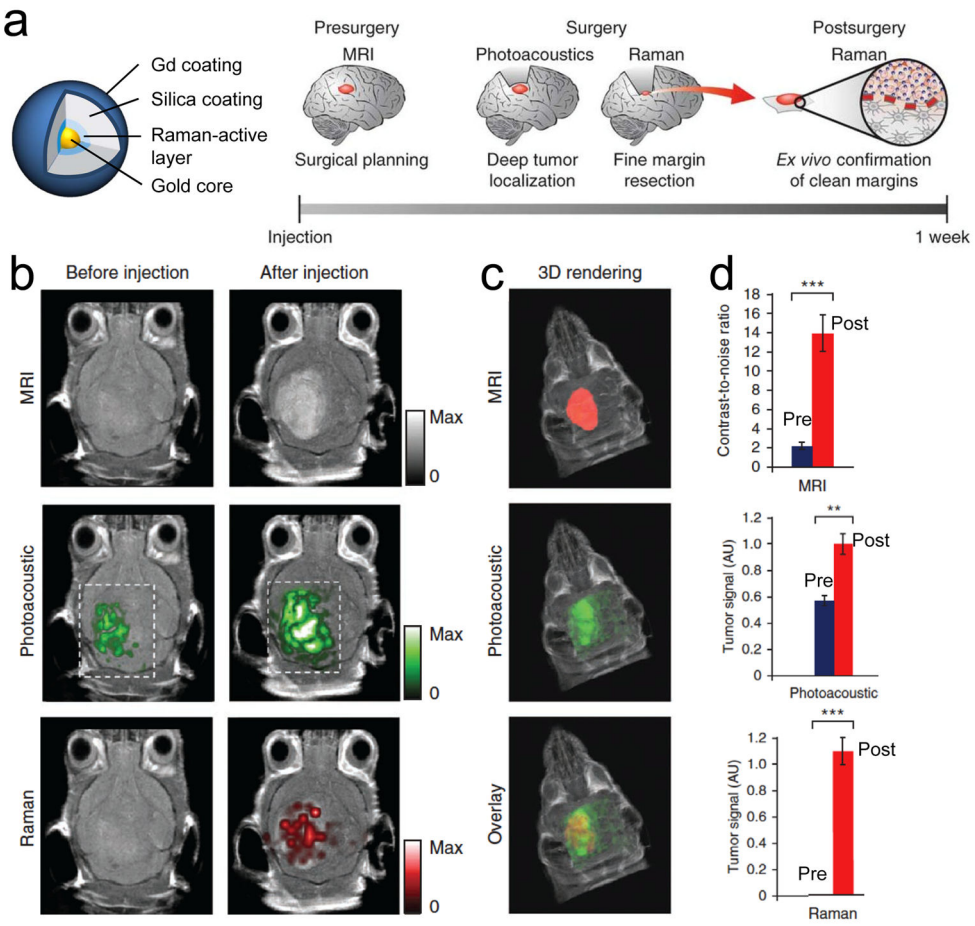

Figure 10.

Brain tumor detection using trimodalities in living mice. a) Chemical structure of trimodal nanoparticles and experimental scheme. b) 2D axial MRI, photoacoustic and Raman images. c) 3D rendering of the segmented tumor with MRI (red; top), photoacoustic (green; middle), and their merged image (bottom). d) Quantitative analysis of tumor signals pre- and postinjection of trimodal nanoprobes ($n = 4$). $^{**}p < 0.01$, $^{***}p < 0.001$ (one-sided Student's *t*-test). AU, arbitrary units. Reproduced with permission.[115] Copyright 2012, Springer Nature.

Table 1

Clinically available fluorophores for fluorescence-guided brain surgery.[64]

Fluorophore	Sodium fluorescein	PpIX (5-ALA-induced)	ICG sodium iodide
Wavelength (Ex)	494 nm	405 nm	805 nm
Wavelength (Em)	521 nm	635 nm	825 nm
Dose	8–10 mg kg^{-1}	20 mg kg^{-1}	0.3 mg kg^{-1}
Admin route, imaging time	Intravenous, 5 min	Oral, 2 h	Intravenous, 15 min
Localization	Extracellular, intravascular	Intracellular	Intravascular
Targeting route	Perfusion	Biosynthesis	EPR
Specificity	NA	>95%	>90%
Advantages	Colorimetric separation	BBB permeability, brain tumor biopsy	Negligible autofluorescence
Disadvantages	Rapid photobleaching, nonspecific high background uptake, possible extravasation along with edema	Porphyria, phototoxicity, low specificity, low sensitivity, high false-negative rates	Nonspecific liver uptake, iodine allergy, liver disease, uremia
Adverse reactions	Nausea and vomiting, anaphylaxis, death	Photosensitivity, nausea, hypertension	Anaphylactic or urticarial reactions